Anal Bioanal Chem (2009) 395:519–525
DOI 10.1007/s00216-009-2952-0

ORIGINAL PAPER

Depolymerization study of sodium hyaluronate by flow field-flow fractionation/multiangle light scattering

Ji Hye Kwon · Euijin Hwang · Il-Hwan Cho · Myeong Hee Moon

Received: 6 May 2009 / Revised: 24 June 2009 / Accepted: 1 July 2009 / Published online: 1 August 2009

Abstract Thermal depolymerization of ultrahigh-molecular-weight (UHMW) sodium hyaluronate (NaHA) was studied systematically by using frit-inlet asymmetrical flow field-flow fractionation/multiangle light scattering/differential refractive index (FI-AFlFFF/MALS/DRI). FI-AFlFFF was utilized for the size separation of NaHA samples which had been thermally degraded for varied treatment times, followed by light-scattering detection to determine MW and structural information of degraded NaHA products. Analysis of NaHA products showed time-dependent depolymerization of raw molecules into smaller-MW components, as well as unfolding of compact structures of UHMW NaHA. To determine whether the observed decrease in MW of sodium hyaluronate originated from the chain degradation of UHMW molecules or from dissociation of entangled complex particles that may have been formed by intermolecular association, narrow size fractions (1×10^7–6×10^7 and $>6\times10^7$ MW) of NaHA molecules were collected during FlFFF separation and followed by thermal treatment. Subsequent FI-AFlFFF/MALS analysis of collected fractions after thermal treatment suggested that the ultrahigh-MW region ($>10^7$ Da) of NaHA is likely to result from supermolecular structures formed by aggregation of large molecules.

J. H. Kwon · M. H. Moon (✉)
Department of Chemistry, Yonsei University,
Seoul 120-749, South Korea
e-mail: mhmoon@yonsei.ac.kr

E. Hwang · I.-H. Cho
Department of Biotechnology,
Shinpoong Pharmaceutical, Co. Ltd.,
Ansan, Kyeonggi-Do, South Korea

Keywords Flow field-flow fractionation · Multiangle light scattering · Sodium hyaluronate · Depolymerization · Biopolymers · Separations/instrumentation

Introduction

Hyaluronic acid (HA) is a natural polysaccharide with a disaccharide repeating unit, [(1→3)-*O*-(2-acetamido-2deoxy-β-D-glucopyranosyl)–(1→4)-*O*-β-D-glucopyranuronosyl]. HA is found naturally in the skin, synovial fluid, umbilical cord, vitreous humor, human cartilage, and rooster comb, and can also be obtained using microbiological methods [1–4]. Biologically, it plays an important role in both mechanical and transport systems in the body. Solutions of sodium hyaluronate (NaHA) or hyaluronan, a sodium salt of hyaluronic acid (HA), have versatile uses in ophthalmic surgery and arthritis treatment with relatively high-MW molecules ($>1\times10^6$), and in wound repair and cosmetological applications with lower MW species ($<1\times10^6$), due to the biologically safe nature and characteristic properties of the material [5–10]. Depolymerization of ultrahigh-MW NaHA materials into lower MW materials has been commonly utilized for the applications described above. NaHA polysaccharide chains can be readily degraded into smaller-MW compounds by simple physical or chemical processes such as heating, irradiation with gamma rays, enzymatic hydrolysis, oxidation, and membrane filtration [10–13].

NaHA forms a worm-like coil in dilute solution [2, 14] or multiple helical structures that are stabilized by hydrogen bonds between glycosidic-linked monomers in the solid state [15]. It has also been reported that transient hyaluronate networks arise from intra-chain hydrogen-bonding interactions between stiff segments in sodium chloride

solution [16]. Most of these studies on HA structure utilized low-angle X-ray and viscometric analysis with small NaHA molecules.

FlFFF, an elution technique to fractionate macromolecules by hydrodynamic diameter, has been utilized for size characterization of particles, proteins, and water-soluble polymers [17–21]. FlFFF, a variant of field-flow fractionation (FFF) techniques, utilizes a crossflow stream as an external force perpendicular to the migration flow, which moves along the channel axis driving sample molecules to the detector. Since FlFFF separation is carried out in a thin unobstructed channel, it reduces or bypasses the possible adsorption of sample components on packing materials, shear degradation of large-MW polymers, or column blocking, which can occur when conventional size-exclusion chromatography (SEC) with spectrometric or viscometric analysis is utilized for the characterization of soluble polymers [22]. When FlFFF is combined with multiangle light scattering (MALS) and a differential refractive index (DRI) detector, it provides an independent measurement of molecular weight and molecular weight distribution of a broad-molecular-weight-polymer sample, along with conformational information. On-line FlFFF-MALS has been utilized for the separation and size characterization of aqueous polymers [23–26]. It has been recently applied to purified NaHA materials [2] and degradation products, obtained by various processes such as ultrasonication, gamma ray irradiation, and enzymatic reactions [27–30].

In this study, FlFFF-MALS was utilized to study the systematic change in sizes and conformation of NaHA samples that had been treated by heat. MW distributions and structural differences of NaHA products were compared in relation to the thermal treatment periods. To understand more about depolymerization of NaHA during thermal treatment, ultrahigh-MW fractions of NaHA were collected during repeated FlFFF separations of raw NaHA material. The FlFFF fractions, collected at narrow-MW intervals, were thermally treated in a similar way (100 °C) used for the treatment of bulk material and then analyzed with FlFFF-MALS to discover whether low-MW NaHA molecules originate from the disentanglement of NaHA networks (by agglomerization of several molecules) or from depolymerization of individual ultrahigh-MW NaHA molecules.

Experimental

Materials and reagents

Raw sodium hyaluronate samples were extracted from rooster comb and thermally treated by Shinpoong Pharmaceutical Company, Ltd. (Ansan, Korea). Thermal depolymerization occurred by heating the raw NaHA solution (at a concentration of 10 g/L in 0.3 M NaCl solution) at 100 °C for varying time periods: 5, 10, 15, 20, 25, and 30 min. The heat-treated NaHA samples were diluted in 0.1 M $NaNO_3$, at a concentration of 0.8–1.0 mg/mL, and held at 4 °C overnight without stirring in order to prevent degradation. The carrier solution used for frit-inlet asymmetrical flow field-flow fractionation (FI-AFlFFF) separation in this study was 0.1 M $NaNO_3$. For thermal treatment of the narrow-MW NaHA fractions collected during FI-AFlFFF separation, each collected fraction was first desalted using a Spectra/Por 3.5 kDa dialysis membrane kit from Spectrum Laboratories, Inc. (Rancho Dominguez, CA, USA) overnight in a water solution. After dialysis, the resulting NaHA fractions were freeze-dried and re-dispersed in the carrier solution for further analysis with FI-AFlFFF.

To prepare depolymerized NaHA products by membrane filtration, the same raw NaHA solution (0.6 g/L) was filtered through a cartridge filter 0.22 μm Hydrophilic Durapore from Millipore Corp. (Billerica, MA, USA) with a pressure of 2 kgf/cm^2. After filtration, the filtrate was stored at 4 °C for direct analysis by FI-AFlFFF without lyophilizing.

FFF/MALS/DRI

The FI-AFlFFF channel employed in this study was similar to the one reported in previous studies [27, 28]. The channel space was made by cutting a 178-μm-thick Mylar spacer with a tip-to-tip length of 28.3 cm. The channel had a trapezoidal shape (the initial breadth decreased from 2.0 to 1.0 cm), and the geometrical volume of the channel was 0.70 cm^3. The FI-AFlFFF channel was constructed by clamping the spacer with two plastic blocks. One wall, the accumulation wall, had a ceramic frit covering the whole channel space to allow for crossflow to pass through. The other wall, the depletion wall, had a small frit (3.0 cm from the channel inlet) at the channel inlet area. A high-speed frit flow was introduced to the channel through the small inlet frit, at the same time as sample components were introduced through the channel inlet at a very low speed (usually 0.1 mL/min). The role of the frit flow was to provide hydrodynamic relaxation [31, 32] of incoming sample components without stopping the migration, which was typically required in conventional FlFFF channels. When the two channel blocks were bound together, a PLCGC regenerated cellulose membrane (20 kDa MWCO) from Millipore Corp. (Billerica, MA, USA) was placed at the accumulation wall side.

For the delivery of carrier solution (0.1 M $NaNO_3$ solution prepared from deionized water), two HPLC pumps were utilized: a Model 305 HPLC pump from Gilson (Villers Le Bell, France) for sample injection through the

sample inlet of the channel and a Model M930 HPLC pump from Young-Lin Co. (Seoul, Korea) for the frit flow through the inlet frit. Flow-rate programming of frit flow [33] was made with the latter pump in a multistep linear decay pattern: the initial frit-flow rate (set as identical to crossflow rate in this study) began at 2.0 mL/min for 4 min and then decreased linearly to 0.5 mL/min over 5 min, to 0.1 mL/min over 7 min, further to 0.02 mL/min over 9 min and then, finally, was maintained at 0.02 mL/min until the end of separation. During crossflow programming, crossflow was circulated by connection to the inlet of the frit-flow pump. The rate of outflow leading to the detector was maintained at 0.1 mL/min throughout each separation. A syringe pump, Model PN1610 Syringe Dosing System from Postnova Analytics (Lansberg, Germany), was utilized in unpump mode at the end of the detector for accurate control of flow rate.

For monitoring eluted NaHA molecules, two serial detectors were employed: a DAWN-DSP multiangle light-scattering detector from Wyatt Technology (Santa Barbara, CA, USA) at a wavelength of 632.8 nm for the first detection, and an Optilab DSP differential refractive index (DRI) detector from Wyatt Technology at a wavelength of 690 nm. Calibration and normalization of MALS were performed with filtered toluene and albumin, respectively. Data collection and MW calculation of eluted sample components were made with ASTRA software (Wyatt Technology). For MW calculation, the DRI fractogram was baseline-adjusted by subtracting the baseline of each blank run with CORONA software from Wyatt Technology. A third-order polynomial fit according to the Berry method of the Debye plot was utilized with measured d*n*/d*c* value for the NaHA sample. Measurements of d*n*/d*c* of the samples were made with an Optilab DSP interferometric refractometer with respect to concentration variation using the same carrier solution (0.1 M $NaNO_3$), and calculated with DNDC5 software (Wyatt Technology). The measured value of d*n*/d*c* was 0.184 for the raw NaHA sample utilized in this study.

Results and discussion

The raw NaHA sample and six depolymerized NaHA products dispersed in 0.1 M $NaNO_3$ solution were examined by FlFFF-MALS using the crossflow programming method. Figure 1 shows superimposed LS signals (90°) from the control (raw material) and three thermally treated samples (with thermal depolymerization of 10, 20, and 30 min) along with DRI signals obtained during FlFFF separation. The LS signals of the control sample appear as a broader distribution, through a longer time span, and with higher intensity than signals of the three thermally treated

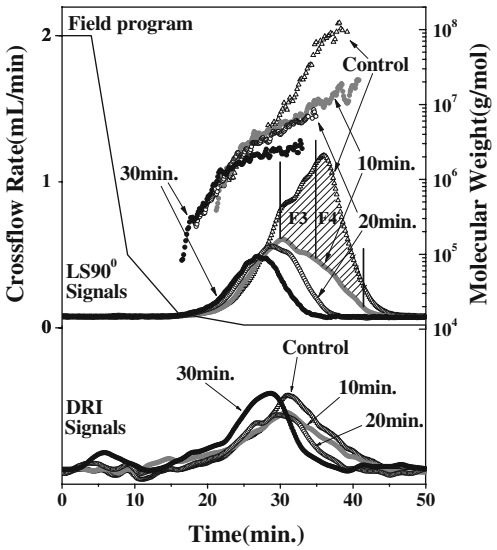

Fig. 1 FlFFF fractograms (DRI signals at the bottom and MALS at 90°) of NaHA samples (control sample and three thermally treated samples) and MW values calculated at each retention time slice. FlFFF separation was carried out using a field decay program for varying crossflow rates over time and at a fixed outflow rate of 0.10 mL/min. Fractions F3 and F4 were collected during the separation of the control sample for separate thermal treatment. The *solid line* represents the field programming pattern scaled with the crossflow rate at the *left axis*

samples, because light scattering depends on both MW and concentration. As the period of thermal treatment increased from 10 to 30 min, retention of the treated sample shifted toward the shorter time scale, indicating a decrease in MW, and peak intensity decreased simultaneously. MW values calculated at each time slice are marked with the same symbols corresponding to each fractogram. The calculated MW values of the control NaHA sample exhibited a broad MW distribution ($10^6 \sim 10^8$ Da) as well as a gradual increase in MW as retention time increased, showing that FlFFF separation was successful up to 10^8 Da. The LS signal of the 10-min-treated sample (marked with gray circles) showed a similar MW pattern at the beginning of elution (20–30 min), but MW values at later elution times (>30 min) appeared to be clearly different from the MW ($>6\times10^7$ Da) found in the control sample. This difference can be explained by the difference in FlFFF retention of differently shaped materials: linear molecules are retained longer than spherical molecules of the same MW. There is also a possibility that very large molecules or aggregates co-elute in the steric mode of FFF after 30 min of retention. If ultrahigh-MW NaHA molecules ($>6\times10^7$ Da) are disentangled or depolymerized by thermal treatment, they exhibit relatively more extended structures. As the thermal treatment period increased to 30 min, the MW distribution shifted to a much smaller region with narrower distribution. The change in MWD with the increase of treatment period

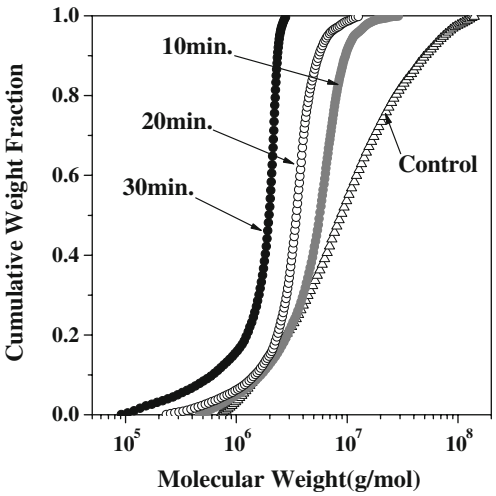

Fig. 2 Molecular-weight distributions of the four NaHA samples before and after thermal treatment

is compared in Fig. 2. It is noted in Fig. 2 that with 10 or 20 min of thermal treatments, populations of ultrahigh-MW species seem to disappear, while those of smaller species (less than 10^6 Da) do not increase significantly. However, when it is treated with 30 min, low-MW species appear to increase greatly. The weight average MW and radius of gyration values are listed in Table 1, along with data obtained with samples thermally treated for 5, 15, and 25 min, which are not shown in Figs. 1 and 2.

The influence of heat shock on the structure of NaHA molecules in solution can be estimated from the slope of the logarithm plot of root-mean-square (RMS) radius vs. MW values in Fig. 3. The RMS radius-MW plots of the control sample and the 5-min-treated sample in Fig. 3a showed a similar pattern in which RMS radius values increased gradually with MW. However, the ultrahigh-MW region (>10^7 Da) of the control sample showed a shallow increase of RMS radius as MW increased. Thus, slope values were calculated separately in two different regions. The slope value for the lower MW region (<10^7 Da; region II in Fig. 3a) was 0.33. However, it was even smaller (0.15) for ultrahigh-MW region (>10^7 Da; region I in Fig. 3a). The slope value is a good predictor of the structure of molecules in solution: compact (~0.33) and linear (~0.67). Figure 3a also shows that 5 min treatment did not critically alter the structure of NaHA molecules and MWD except for the disappearance of very large molecules (>2×10^7 Da). This result did not demonstrate whether the disappearance of these large molecules was caused by depolymerization, or by disaggregation due to the enhanced dissolution of ultralarge molecules by a short period (5 min) of heat treatment. This was addressed with more experiments. Figure 3b and c compared the RMS radius-MW plots of the other five depolymerized samples. As the treatment period increased, the slope value increased to 0.39, 0.43, 0.45, and 0.59 for the samples treated with 15, 20, 25, and 30 min, respectively, showing that NaHA molecules during thermal treatment transitioned to extended structures. Upon 30 min of thermal treatment, NaHA molecules appear to be nearly linear in structure, with an increase of population at the small-MW region (<10^6 Da). Figure 3 suggests that thermal treatment of NaHA of less than 10 min did not alter the molecules' structure clearly, although the ultrahigh-MW molecules disappeared. However, after 20 minutes of treatment, the molecules began a structural unfolding, indicated by comparing the slope values.

In order to discern whether the ultrahigh-MW fraction of the raw material was broken into smaller pieces or disaggregated during thermal treatment, we collected two narrow but ultrahigh-MW fractions during FlFFF separation of the raw NaHA material, at time intervals marked in Fig. 1 (F3, 30–35 min. and F4, 35–41 min), for size-specific thermal treatment followed by FlFFF-MALS analysis. The collected fractions were accumulated by repeating injections 20 times, and the resulting fractions were treated for 20 min at 100 °C and called F3/T and F4/T. The two fractions were run at the same experimental condition used for Fig. 1. Figure 4 shows the comparison of MALS signals of the collected fractions (F3 and F4)

Table 1 Calculated Mw, Mn, RMS radius, and slope values of the thermally treated NaHA samples compared with the control sample

	Mw(g/mol)	Mn(g/mol)	Mw/Mn	RMS radius (nm)		Slope	Slope error
				Rw	Rn		
Control	$(1.92\pm0.04)\times10^7$	$(4.89\pm0.07)\times10^6$	3.92±0.10	142.3±0.6	104.3±0.4	0.30	0.005
5 min	$(7.91\pm0.11)\times10^6$	$(4.26\pm0.05)\times10^6$	1.86±0.03	119.7±0.5	104.5±0.4	0.31	0.007
10 min	$(5.77\pm0.07)\times10^6$	$(3.40\pm0.04)\times10^6$	1.68±0.03	111.9±0.5	96.8±0.5	0.33	0.005
15 min	$(4.40\pm0.04)\times10^6$	$(3.97\pm0.04)\times10^6$	1.11±0.01	97.0±0.3	92.9±0.3	0.39	0.004
20 min	$(3.90\pm0.03)\times10^6$	$(3.27\pm0.02)\times10^6$	1.19±0.01	95.2±0.3	77.5±0.4	0.43	0.004
25 min	$(2.76\pm0.02)\times10^6$	$(1.59\pm0.02)\times10^6$	1.73±0.02	94.9±0.4	76.0±0.5	0.45	0.006
30 min	$(1.76\pm0.01)\times10^6$	$(1.59\pm0.01)\times10^6$	1.65±0.02	87.0±0.3	68.0±0.4	0.59	0.011

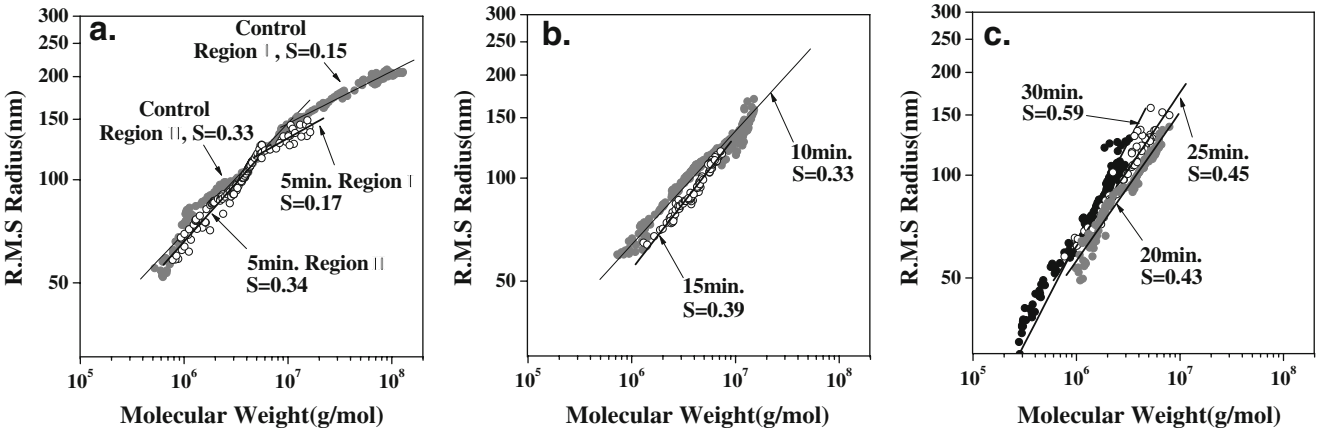

Fig. 3 Plots of RMS radius vs. MW values of thermally treated samples. **a** The control and the 5-min-treated sample, **b** 10- and 15-min-treated samples, and **c** 20-, 25-, and 30-min-treated samples

before and after thermal treatment (F3/T and F4/T) along with cumulative MW distribution curves and the plot of logarithm of RMS vs. logarithm of MW for each treated fraction. Fractograms of the two re-injected fractions (F3 and F4) without thermal treatment are different from each other in the smaller-MW regime (<10^7 Da) in Fig. 4a while both fractions contain some portion of the very-large-MW species. After thermal treatment, LS signals of F3/T and F4/T appear to be shifted toward the shorter retention time scale along with broader distribution, however, the two fractograms of the lower part of Fig. 4a are similar to each other in retention times, with a slight difference in the calculated MW values. The calculated MW values, plotted above the MALS signals in Fig. 4a, indicate that the two fractions apparently contain molecules larger than 10^7 Da. However, the cumulative distribution curves (Fig. 4b) show that the relative amount of the large-MW portion of both fractions is less than 10% in weight. In addition, the relative amount of smaller-MW (<10^6 Da) species is low for the two thermally treated fractions, compared to the 30-min-treated raw sample (shown in Fig. 1a). The absence of such smaller species in the collected fractions after 20 min of treatment suggests that depolymerization or chain degradation from ultrahigh-MW fraction of NaHA at the given treatment time (20 min) is not likely to be a contributing factor to the size reductions observed for the two fractions

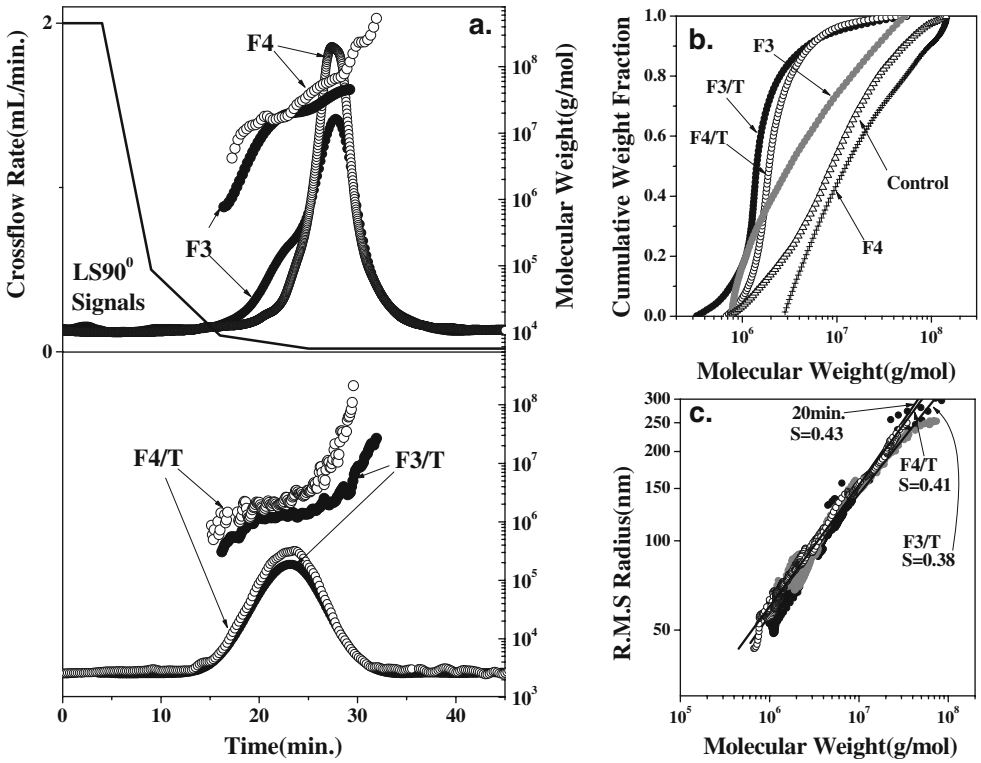

Fig. 4 **a** Comparison of LS signals of re-injected FlFFF fractions before (F3 and F4 marked in Fig. 1) and after thermal treatment (F3/T and F4/T), **b** the superimposed plot of cumulative distribution curves of each fraction including the control sample, and **c** plots of RMS radius vs. MW values of the thermally treated fractions, F3/T and F4/T

Table 2 Calculated Mw, Mn, RMS radius, and slope values of the thermally treated fractions, F3/T and F4/T, which were collected during the separation of the control sample marked in Fig. 1

	Mw(g/mol)	Mn(g/mol)	Mw/Mn	RMS Radius(nm)		Slope	Slope error
				Rw	Rn		
F3/T	$(8.03\pm0.16)\times10^5$	$(3.10\pm0.05)\times10^5$	2.60±0.07	138.1±1.2	103.1±1.2	0.41	0.002
F4/T	$(2.95\pm0.09)\times10^6$	$(7.05\pm0.16)\times10^5$	4.18±0.15	146.6±1.2	113.9±1.4	0.38	0.004

(F3/T and F4/T). It can be explained more with the experimental finding in Fig. 4b that population of smaller-MW species ($<1\times10^6$ Da) is not significantly increased while the population of ultrahigh-MW molecules decreases for the two treated fractions. A similar observation is also found in Fig. 2 that smaller-MW species for the 10- or 20-min-treated samples did not increase as much as the observed decrease of ultrahigh-MW species. Moreover, the molecular structures estimated from the RMS vs. MW plot for the two fractions (F3/T and F4/T) are comparable to that of the 20-min-treated raw sample in Fig. 4c. This also suggests that the three samples may exhibit a similar structure, judged from their similar slope values. These observations suggest that the ultrahigh-MW region ($>10^7$ Da) of NaHA shown in Fig. 1a may originate from supermolecular structures formed by aggregation of large molecules, supporting multi-fold helical structures, which was suggested by an earlier work [15]. Calculated MW and MN values of the two fractions after thermal treatment are listed in Table 2.

A similar mechanical process using membrane filtration also resulted in a decrease in MW. When the same raw material was filtered through a membrane filter with 0.2 μm pores, the result was in a significant decrease in MW, very similar to that seen from 25 and 30-min thermal treatments. The cumulative distribution curve of the filtered sample was compared with those of the 25- and 30-min depolymerized samples along with that of the control sample, showing that MWD fell between those of the two samples (Fig. 5a) and the slope value (0.50) does too (Fig. 5b). However, about 30% of the weight distribution of the products of membrane filtration were smaller species ($<10^6$ Da), while the two thermally treated samples showed only about 15% of these smaller species.

Conclusions

In this study, influence of thermal treatment of water-soluble NaHA raw material on depolymerization was systematically examined using FlFFF-MALS. Thermal treatment of sodium hyaluronate for a short period of time (up to 10 min at 100 °C) brought a minor change in molecular-weight distribution, due to the enhanced dissolution of ultralarge MW NaHA molecules in water without a significant change in structure. However, when thermal treatment was longer than 10 min, there was a serious reduction of average molecular weight, as well as unfolding of complicated geometry, which suggested the depolymerization of NaHA molecules. FlFFF-MALS analysis of two thermally treated fractions collected in a narrow but ultrahigh-MW region during FlFFF run of the raw material suggested that the presence of ultralarge molecules ($>10^7$ Da) may be from supermolecular structure caused by aggregated species or poorly dissolved species.

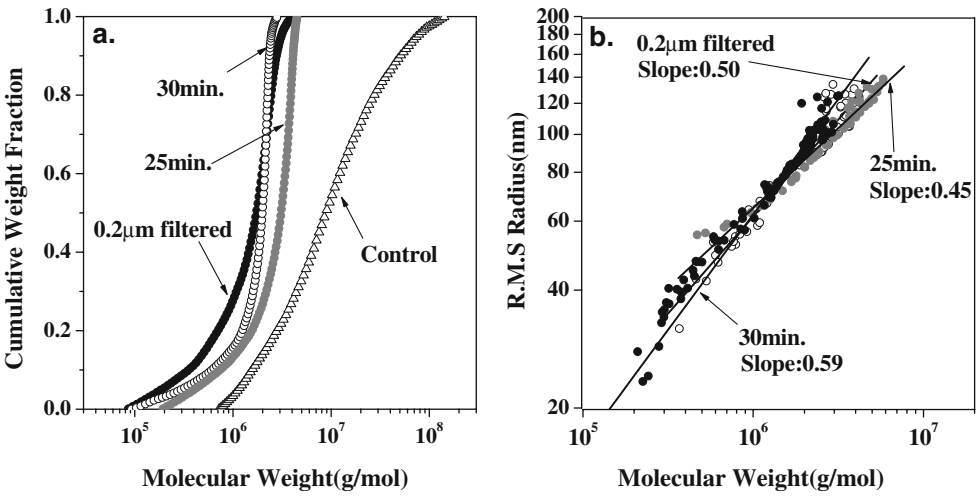

Fig. 5 **a** Plots of RMS radius vs. MW values of the NaHA sample treated by membrane filtration compared with the thermally treated samples (25 and 30 min) and **b** the comparison of the cumulative distribution curves

Acknowledgements This study was supported by the Korea Science and Engineering Foundation through the Center for Bioactive Molecular Hybrids (CBMH) at Yonsei University and in part by Shinpoong Pharmaceutical, Co. Ltd.

References

1. Cortivo R, Brun P, Rastrelli A, Abatangelo G (1991) Biomaterials 12:727–730
2. Prestwitch GD, Marecak DM, Marecek JF, Vercurysse KP, Ziebel MR (1998) J Controlled Release 53:93–103
3. Iqbal Z, Midgley JM, Watson DG, Karditsas SD, Dutton GN, Wilson W (1997) Pharmacy World & Science 19:246–250
4. Vercruysse KP, Prestwich GD (1998) Crit Rev Ther Drug Carrier Syst 15:513–555
5. Sasari H, Konttinen TY, Santavirta S (1989) Med Sci Res 18:99–101
6. Takahashi R, Al-Assaf S, Williams PA, Kubota K, Okamoto A, Nishinari K (2003) Biomacromolecules 4:404–409
7. Mengher LS, Pandher KS, Bron AJ, Davey CC (1986) Br J Opthalmol 70:442–447
8. Miyazaki S, Yomota C, Okada S (1996) J Ocul Pharmacol 12:27
9. Yeung B, Marecak D (1999) J Chromatogr A 852:573–581
10. Rehakova M, Bakos D, Soldan M, Vizarova K (1994) Int J Biol Macromol 16:121–124
11. Sall I, Ferad G (2007) Polym Degrad Stab 92:915–919
12. Ynag BY, Montgomery R (2007) Bioresour Tech 98:3084–3089
13. Soltes L, Mendichi R, Kogan G, Schiller J, Stankovska M, Arnhold J (2006) Biomacromolecules 7:659–668
14. Cleland RL (1977) Arch Biochem Biophys 180:57–68
15. Livant P, Roden L, Krishna R (1992) Carbohydr Res 237:271281
16. Sheehan JK, Arundel C, Phelps CF (1983) Int J Biol Macromol 5:222–228
17. Giddings JC (1981) Anal Chem 53:1170A–1178A
18. Giddings JC (1993) Science 260:1456–1465
19. Wahlund K-G, Giddings JC (1987) Anal Chem 59:1332–1339
20. Ratanathanawongs SK, Giddings JC (1992) Anal Chem 64:6–15
21. Kim H, Lee H, Moon MH (2006) Bull Korean Chem Soc 27:413–418
22. Motohashi N, Nakamichi Y, Mori I, Nishikawa H, Umemoto K (1988) J Chromatogr 435:335–342
23. Hecker B, Fawell PD, Jefferson A, Farrow JB (1999) J Chromatogr A 837:139–151
24. Wittgren B, Wahlund K-G (1997) J Chromatogr A 791:135–149
25. Picton L, Bataille I, Muller G (2000) Carbohydr Polym 42:23–31
26. Duval C, Cerf DL, Picton L, Muller G (2001) J Chromatogr B 753:115–122
27. Shin DY, Hwang EJ, Cho I-H, Moon MH (2007) J Chromatogr A 1160:270–275
28. Moon MH, Shin DY, Lee N, Hwang E, Cho I-H (2008) J Chromatogr B 864:15–21
29. Lee H, Kim H, Moon MH (2005) J Chromatography A 1089:203–210
30. Lee H, Cho I-H, Moon MH (2006) J Chromatography A 1131:185–191
31. Moon MH, Kwon HS, Park I (1997) Anal Chem 69:1436–1440
32. Moon MH, Williams PS, Kwon H (1999) Anal Chem 71:2657–2666
33. Moon MH, Kang D, Hwang I, Williams PS (2002) J Chromatogr A 955:263–272